ARTICLES

Study of Type-A Zeolites. Part 1: Mechanism of He and Ne Encapsulation

Yacov Finkelstein, Avraham Saig, Albert Danon, and Jacob E. Koresh*

Chemistry Division, Nuclear Research Center of the Negev, Beer-Sheva 84190, Israel

Received: March 13, 2003; In Final Form: June 26, 2003

The mechanism of *ambient* pressure encapsulation of He and Ne in the α and β crystalline cages of type-A zeolites is demonstrated. Reversible and highly selective gas admission and entrapment are readily achieved at characteristic temperatures occurring between 77 and 570 K. The permeability of the zeolitic windows is governed by an interplay between the critical diameter of the encapsulate and the effective apertures dimension, which is shown to be strongly dependent on temperature. The blocking state of the zeolitic apertures is determined by a simultaneous thermal activation of both cation mobility and structural dilation/constriction of crystalline windows. Encapsulation in NaA (4A) principally occurs in the β cages of the Sodalite units, whereas the K-exchange form (3A) offers both α and β encapsulations. The effective free aperture dimension of the Ca exchange form (5A) is found to be too large to allow a practical gas enfoldment in either class of cavities, even at 77 K, where only poor encapsulation is observed. The counterion location vs size dependence, known only from crystallographic data, is sensed here for the first time by an encapsulation process, via the manifestation of different aperture occupancy states. While the blocking extent of the wider O_8 windows of the α cages is consistent with the size of exchangeable cations, a reverse correlation is evident for the narrower O_6 windows of the β cages.

Introduction

Controlling the accessibility of crystalline voids to inert gases and selectively entrapping them is an obvious desirable requirement from both experimental and applied perspectives. Additional advantage is gained if such confinement is achieved in a reversible, stable fashion and under nondestructive, as ambient as possible, conditions. For that matter, zeolite molecular sieves,[1−3] which are silicoaluminate crystalline frameworks of extremely regular pore structure and uniform small characteristic apertures, may be considered as potential candidates. In particular, most promising is the synthetic type-A class, available in three grades uniquely differing from one another by their molecular sieving properties. Type 4-, 3- and 5-A, respectively relating to the Na and its K- and Ca-exchanged forms, correspondingly admit species with effective kinetic diameters of up to roughly 4, 3, and 5 Å. Structurally, these microporous crystalline structures are considered as rigid sponge constructions, capable of imbibing large amounts of molecules that are small enough or of the right shape, to penetrate the intracrystalline pores, yet excluding molecules having the "wrong" sizes or shapes. The sieving and selectivity properties of zeolites are strongly related to the presence of exchange cations in the framework and their locations therein. They may occupy sites adjacent to apertures located between one void and the next and, according to their charge, number, size, and location, act as sentinels, effectively barring passage of larger molecules while allowing passage of smaller ones. This familiar sieving property is thus very sensitive to the size of the cationic constituents relative to the dimensions of the zeolite windows. Type A zeolite exhibits two classes of regular voids. The smaller cavities (β cages), having the structure of Sodalite units, can be entered only through their eight O_6-ring faces (i.e., six oxygens ringed in a plane) of ∼ 2.3 Å free diameter.[4−7] The second class (α cages) possess larger cavities comprising six O_8 circumferential windows and share eight O_6 windows of eight joint β cages. Every window of each α cage is partly blocked by a sentinel counterion,[7−9] due to which its effective aperture free dimension, and thus the access to its inner available free volume, varies between 3 and 5 Å, whence the terms 3A, 4A, and 5A.

The phenomenon of type A zeolitic encapsulation was studied to some detail in relation to the potential of molecular sieves to serve as storage mediums for inert gases.[6,9−16] Sorption procedures were performed in these studies under practical vitrifying conditions, between 300 and 800 °C and 40 to 1000 bar, at which the zeolite irreversibly turns into an amorphous glassy form with an almost complete loss of its specific surface area.[14] We have recently reported on the first observation of a reversible room-temperature encapsulation of He and Ne in the β cages of NaA following a nondestructive sorption procedure taken at *atmospheric* pressure and around 200 °C.[17] The β cages were shown to act as tunable gates for a selective and reversible admission and efficient entrapment of He and Ne. The present study complements the previous one with explicit detailed measurements of He and Ne in 3A and 5A, providing a broader insight into the overall physical picture of the mechanism ruling the phenomena of encapsulation in zeolites.

Principle of the TPD-MS−SMB Method

In temperature programmed desorption mass spectrometry (TPD-MS), desorption is generated by programmed heating of

* Corresponding author.

10.1021/jp034644f CCC: $25.00
Published on Web 07/30/2003

a sample under ultrahigh vacuum. The desorbed products are collected into an MS apparatus, ionized therein, and their *m*/*z* values are analyzed. The present study utilizes a modified TPD-MS version that allows measurements to be performed under *atmospheric* pressure.[18] Comprising atmospheric TPD with MS raises, however, an essential problem of coupling between the TPD atmospheric pressure and the 9 orders of magnitude lower pressure required in the MS ion source. This problem is countered by utilizing the method of supersonic molecular beam (SMB).[19] In this method the TPD-MS system is provided with a SMB inlet that incorporates two differentially pumped vacuum compartments with a capillary and a nozzle in between. In this configuration the thermally desorbed species are carried from the TPD reactor to the MS chamber by expanding a carrier gas between the above two compartments via a heated capillary and through a nozzle of ca. 80 μm orifice. The gas, adiabatically expanded through the nozzle into vacuum, turns into a supersonic atomic/molecular beam (of the carrier gas and desorbed species), in which the molecular random thermal energy is converted into a unidirectional mass flow. The central portion of the free jet is then sampled with a skimmer (a sharp cone collimator) and utilized for MS analysis.

Experimental Section

A detailed description of the experimental setup is given in ref 18. Sorption and TPD acquisition procedures were reported in ref 17. In each experiment, around 300 mg of as purchased type-A zeolite was introduced into the TPD reactor. The grades used were 1/16 in. 3A and 4A pellets, and 8−12 mesh 5A spheres, manufactured by BDH, Sigma, and J. T. Baker Chemical Co. respectively. All measurements were performed following sample dehydration by evacuating at 295 °C for ca. 24 h, following passive preliminary backing at 250 °C for 3 h in a standard laboratory oven. All sorption procedures utilized either 50 or 20 sccm of UHP He or Ne, respectively, as carrier gases. Two different sets of sorption procedures were performed. In the first, hereby designated as the "static" procedure, gas was introduced to samples cooled in advance to liquid nitrogen (LN_2) temperature by immersing the sorption cell into a LN_2 dewar. However, a temperature of −196 °C could not be reached under vacuum due to poor heat conduction, and only a temperature of ca −176 °C could be attained. Only upon gas introduction did the heat conduction improve, and the sample temperature had dropped down to −196 °C. Thus, in the TPD "static" runs, gas was actually introduced to samples at −176 °C and not −196 °C. In the second sorption procedure, designated as the "dynamic" one; gas was introduced *during sample cooling* from 300 °C to −196 °C. Each sorption procedure was followed by evacuation of excess gas at LN_2, for periods exceeding those of sorption. TPD was then performed by linearly ramping the sample temperature at a constant rate of 20 °C/min. The desorbed products, carried by the inert carrier gas (using He in the case of Ne sorption and vice versa) were probed with a Balzers QMG-422 quadrupole-mass spectrometer (QMS).

To establish optimal static sorption conditions, i.e., to introduce the gas to sample precooled to the lowest attainable temperature of LN_2, a conventional volumetric system was used where three independent measurements were carried out for each sample. The first two simulated the pair of TPD sorption procedures (static and dynamic), i.e., ca. 1000 Torr of gas was introduced to (*i*) evacuated samples precooled to LN_2 by immersion of the sample reactor in LN_2 (static sorption) and (*ii*) during sample cooling (dynamic sorption). As mentioned above, under the static sorption conditions, the actual temperature of the samples was ∼ −176 °C upon gas introduction. In a third modified static sorption version, samples were initially exposed to ∼1 Torr of He (Ne) prior to the introduction of the whole 1000 Torr of Ne (He) probe gas. By doing so, optimal static sorption procedures were achieved, where gas was actually introduced to samples at −196 °C and not only at −176 °C.

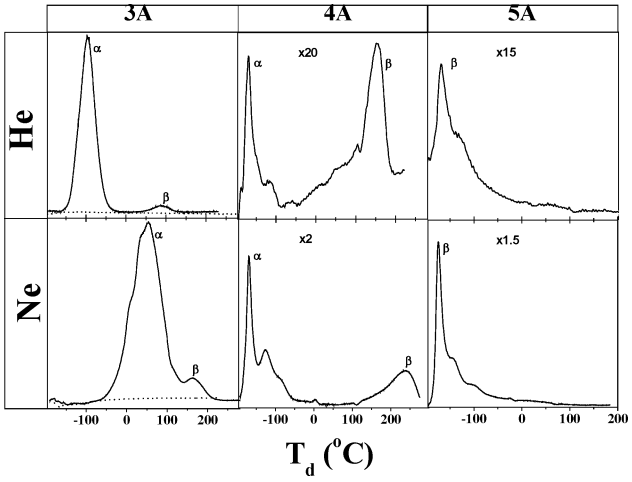

Figure 1. Temperature programmed decapsulation profiles (QMS signal versus sample temperature) of He, upper panel, and of Ne, lower panel, from 3A, 4A, and 5A zeolites, following "dynamic" sorption between 280 °C and LN_2. Dotted curves in 3A depict the results of the "static" sorption taken at − 176 C°. The decapsulation profiles of 4A and 5A are scaled with respect to that of 3A. α and β denote encapsulations in α and β cages, respectively.

Results and Discussion

The phenomenon of encapsulation in 4A was recently proposed[17] to comprise three principal successive steps: (*i*) thermal dilation of zeolitic windows, (*ii*) admission of the gas to the free volume of the cage through its dilated windows, and (*iii*) cooling the gas-loaded sample to LN_2 for an effective aperture closure by thermal contraction and consequent gas entrapment. In the present study the occurrence of He and Ne encapsulation in the crystalline cages of 3A and 5A Zeolites was also confirmed by comparing the TPD profiles following the "dynamic" and "static" sorption procedures. In the dynamic procedure, gas was flown over the sample *during* its cooling between 295 and −196°C, whereas in the static procedure gas was flown over the sample only *after* its temperature was stabilized at LN_2. For all grades, the dynamic sorption procedures produced TPD spectra containing characteristic desorption peaks. In contrast with the above, TPD profiles acquired for the same grades, but following static sorption procedures, were practically flat, evidently indicating the encapsulation of He and Ne, occurring during the dynamic sorption procedure. Typical background subtracted TPD curves measured for the three A-zeolite grades following "dynamic" sorption of He and Ne are shown in Figure 1 (solid curves). To illustrate the inaccessibility of gas due to aperture closure at LN_2, also shown in Figure 1, are representative TPD curves produced following "static" sorption of He on 3A (dotted curves). Reproducibility and precision of data were found to be practically perfect, following comparative measurements among and within various randomly selected samples. We hereby refer to the "dynamic" TPD profiles as those of temperature programmed decapsulation (TPD_c). In general, the curves are shown to have a characteristic structure containing desorption peaks, in the ∼ −170 to 260 °C temperature range. For a given gas type, the decapsulation

profiles of 4A and 5A are equally scaled with respect to that of 3A (scaling factors are depicted in Figure 1). The apparent unexpected occurrence of He and Ne "desorption" peaks at noncryogenic temperatures, particularly above room temperature (see 3A and 4A curves in Figure 1), is attributed to the occurrence of a decapsulation process and not ordinary desorption.[17] Basically, the encapsulation phenomenon occurs due to a significant flexibility of the zeolitic skeleton,[20−22] which allows its windows to undergo thermal dilation/contraction. Gas is admitted via thermal dilation and may then undergo firm enfoldment by thermal contraction of the initially dilated apertures. Discharge of encapsulated gas from its hosting cage may then be achieved by reheating. As discussed below, the TPD_c peaks in Figure 1 can be assigned to decapsulations from individual classes of cages (α or β) in which gas is accommodated and entrapped by purely accounting for dimensional considerations, i.e., the free aperture dimensions and the critical diameters of admitted gas.

The background subtracted profiles of 4A and 5A (Figure 1) depict the occurrence of a small structured peak near LN_2, centered at about −170 °C, whereas in 3A the low-T peak is shifted toward higher temperatures. This result seems to be in accordance with the expected better closure of its apertures with respect to those in 4A and 5A. A further support for this may be gained by the fact that the 4A and 5A low-T peaks are smaller by factors of ca. 20 and 2 for He and Ne respectively, as compared with the 3A low-T peak. All together, such a raw observation could imply the occurrence of poor low-T encapsulations in 4A and 5A, in the sense that the closure of the relevant windows in these grades is incomplete for the entrapment of He and Ne, even at temperatures as low as LN_2. Still, the above observation cannot provide a solid clue for the occurrence of low-T encapsulation in 4A and 5A. In the case of 3A, the TPD peaks are attributed to those of decapsulation due to the flat TPD profile recorded following the static sorption (dotted curves in the 3A panel of Figure 1). The same argument was used to establish the high-T peaks of 4A to those of decapsulation, where for $T > 0$ °C, the TPD curves of 4A following static sorption were indeed flat. Nevertheless, a similar unambiguous consequence could not be concluded for the low-T peaks of the 4A and 5A grades. This is due to the lowest attainable temperature of only −176 °C occurring in the TPD sorption setup (see Experimental Section). To establish that the low-T peaks in 4A and 5A are indeed decapsulation peaks, it was necessary to carry an optimal static sorption, i.e., one in which gas will be introduced to the sample at −196 °C. The differences between the two versions of the static sorption experiment were accounted for by utilizing the volumetric measurements. The volumetric experiments simulating the TPD sorption procedures fully reconstructed those observed in all TPD measurements. Nonetheless, for 4A and 5A, essential differences were observed between the two versions of the static volumetric runs. As predicted, in the optimal static runs negligible amounts of decapsulated Ne and He, smaller by more than 1 order of magnitude with respect to those released in the defective static sorption, were detected upon reheating, clearly signifying a better aperture closure at −196 °C than at − 176 °C. This result, which may be viewed as the equivalent for flat TPD profiles that would be expected following a real static sorption, confirms the occurrence of encapsulation in 4A and 5A at low *T*.

It may be seen in Figure 1 that while the TPDc profiles of 4A contain two principal decapsulation peaks, those of 5A possess only a single low-T decapsulation peak. The occurrence

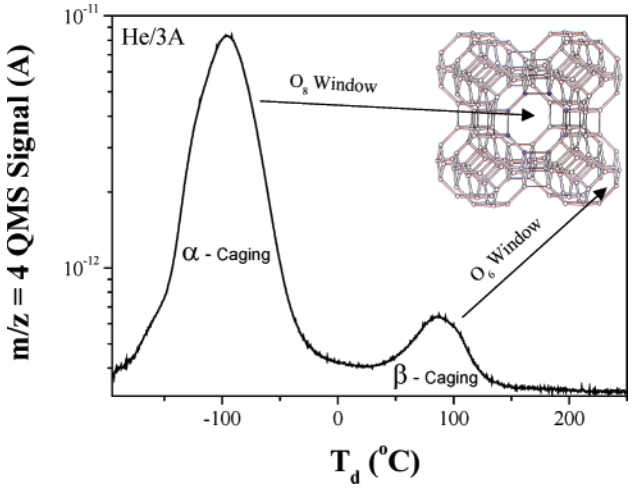

Figure 2. Decapsulation peak assignments. The profile is a logarithmic presentation of a typical He/3A TPD spectrum taken following "dynamic" sorption procedure between 280 °C and LN_2. α and β decapsulation peaks are attributed to gas release through the O_6 and O_8 windows, respectively.

of a single decapsulation peak in 5A may be understood due to the large aperture dimension of ca. 5Å offered by this grade. As a result, cooling a He/Ne loaded 5A sample to LN_2 does not provide sufficient enclosure of the zeolitic windows, even for the larger Ne atom, and gas is easily driven off upon evacuation at LN_2. Since O_6 apertures are smaller than those of the O_8 windows, the sole 5A low-T decapsulation peak may be assigned to a poor β encapsulation.

Far more interesting are the observed differences between the decapsulation profiles of He and Ne from 3A and 4A. The 4A decapsulation peak occurring above RT was previously assigned to entrapment in β cages.[17] The occurrence of high-T decapsulation temperatures of ca. 150 and 250 °C for He and Ne respectively (see Figure 1) originates from the activation energies required for the dilation of the smaller O_6-β apertures, rather than the wider O_8 windows of α cages. Even at −176 °C the O_8 windows are already too widely opened relative to He and Ne, and their transparency for entrapment of these species above RT is obvious. The noted differences between the decapsulation temperatures of He and Ne from 4A depict the occurrence of a highly selective entrapment between them and are in accordance with the differences between the kinetic diameters of He and Ne.

The new results obtained here for 3A practically confirm the concluded β and not α encapsulation (of He and Ne) in NaA Zeolite.[17] The appearance of a second, lower *T* decapsulation peak in 3A strongly suggests the observation of decapsulation from the larger α cavities. Moreover, the involved decapsulation temperatures are consistent with dimensional considerations. While the α free aperture dimension in 4A seems to be too large to allow effective enfoldment of He and Ne, that of 3A clearly meets the "suitable" size for the entrapment of He and Ne atoms. Indeed, only ∼ 50 °C are sufficient for dilating the larger α apertures in 3A, whereas it effectively requires as much as 150 °C to dilate the smaller β apertures for Ne release. Similarly, for the smaller He atom, only ∼90 and ∼ −100 °C are respectively required for decapsulation from the β and α cages. All in all, the 4A and 5A common −170 °C peak, may now be assigned with high certainty to α and β encapsulations, respectively. Figure 2 summarizes the α and β decapsulation assignments established in the present work. It depicts, in a log scale, a typical He/3A TPD spectrum accompanied by a schematic illustration of the α and β cages of a type A zeolite.

The TPD peaks are assigned to the zeolitic O_6 and O_8 windows, according to the above discussion. The fact that He is smaller with respect to Ne results in a perfect resolution of the α and β peaks in the case of 3A.

The most important outcome of the present study concerns the effect of counterions locations on the encapsulation process. Up to now, the net effect of differently occurring encapsulation temperatures for various species in A-zeolite was interpreted as being governed by structural dilation, i.e., thermal activation of the vibrational motion of the O_8 and O_6 apertures through which accesses to the α and β cages are gained. It should be noted, however, that the pore size, shape, and dimensionality of the zeolite are dependent not only on the framework cavities but also on the type of neutralizing cations contained in the nonframework structure. The effective aperture openings could thus be strongly affected by the number, locations, and mobility of the exchangeable counterions (K^+, Na^+, and Ca^{2+} in 3A, 4A and 5A, respectively).[1,2] These zeolites are so termed due to their particular characteristic sieving properties, i.e., O_8-α apertures, whose effective openings limit the admission of species of minimum cross sections of 3, 4, and 5Å respectively.[1−3]

No complete experimental observation was reported so far on a direct detection of the effect counterion mobility has on the effective aperture dimension. As clearly seen in Figure 1, for a given gas type, the α decapsulation peaks are located at higher temperatures relative to those of 4A, in consistency with differences in size of sentinel cations (K^+ is larger than Na^+, thus imposing a relatively stronger blocking effect on the α apertures). This is further supported by considering the locations of α peaks measured for a given grade but different gas type. This is pronouncedly noticed in 3A, where the α peak of Ne shifts toward higher T by more than 150 °C with respect to He.

A similar comparison between the locations of the β peaks depicts, however, an unexpected irregularity, since they systematically occur at higher temperatures in 4A than in 3A, irrespective of gas type. This apparently anomalous result illustrates the fundamental ambiguous effect of cations locations. The apertures of the β cages in 3A are expected to be more effectively blocked relative to those in 4A due to the presence of the larger sentinel K^+ ions. Thus, one expects gas admission to β cages in 3A to occur at higher temperatures relative to those required in the case of the apparently "less blocked" 4A O_6 apertures. Our experimental data clearly imply the opposite, where He and Ne decapsulate from 3A at ∼ 90 and 160 °C respectively, and from 4A only at ∼ 150 and 250 °C (Figure 1). A realistic explanation for the above may be traced out by accounting for the irregularity of cations locations and rearrangements in type A zeolites. The twelve Na^+ cations in dehydrated NaA for example, are arranged such that eight are displaced ca. 0.4 Å from the center of the O_6 windows into the inner volume of the α cage, whereas three are located in the O_8 rings, and about 1.2 Å off center (the remaining sodium is located opposite the 4-ring).[2]

The location of larger univalent cations is believed to occupy the O_8 rings,[1,2,12] which implies that the O_6 windows are left more vacant. In fully exchanged titanium A Zeolite for example, up to eight Ti^+ cations, which are comparable in size to K^+, are located off the plane of the 6-rings, extending ∼ 1.12 Å into the α cage, again favoring the vacancy of the O_6 apertures relative to that in the sodium 4A grade. In 3A, three potassium ions are located near the centers of the O_8 rings, thus restricting their free opening to ca. 3 Å.

In view of the above, the present results are consistent with the "reversed size effect" that the exchangeable cations have on the α and β apertures in zeolite A. O_8 windows comply with the size of exchangeable cations, i.e., their blockage increases with cations size. On the other hand, O_6 windows are differently occupied when small univalent cations are exchanged with larger ones, such that the presence of the latter ones results in the effective widening of the β apertures. It should be noted that this is the first time that the above is experimentally realized via the observation of encapsulation/decapsulation mechanism, rather than by structural diffraction analysis, or theoretical calculations.

A final remark from an applied point of view concerns the effect of quantum sieving (QS). Tailoring porous materials that will provide the first experimental realization of the predicted QS effect was raised quite recently by several theoretical reports.[23,24] The possibility of utilizing zeolitic encapsulation of He and Ne for atomic QS was previously suggested and discussed for the case of β-encapsulation in 4A.[17] The present new results show, however, that 3A, for which practically perfect α/β resolution was obtained for He, suggests that this zeolite grade is, at present, the far most promising candidate available for testing the possible occurrence of atomic QS between ^{3}He and ^{4}He. The effect in such a case is predicted to be very large due to the difference between the isotope−zeolite binding potentials, amounting in the case of ^{3}He and ^{4}He confined in narrow channels, to about 33%.[23]

Conclusions

Ambient pressure encapsulation of He and Ne in type A zeolites was utilized for probing the effective aperture dimensions of the principal building cavities of these crystalline constructions versus temperature between 77 and 570 K. The usage of inert atomic probes enabled a sensitive, pure explicit follow-up of the various mechanisms governing encapsulation, as well as their interplays. The effective O_8 and O_6 aperture openings (of the α and β cages respectively) are shown to be temperature sensitive, confirming the flexibility of the crystalline framework, which allows their thermal dilation/contraction. The results also give clear indications as to the crucial role played by the stabilizing zeolitic counterions as temperature-dependent blocking sentinels. The occurrence of different counterions occupancy states is shown to affect the wider O_8-α windows in consistency with the size of exchangeable cations, while a reverse correlation is evident for the case of the narrower O_6-β apertures. This effect, theoretically predicted and partly shown by crystallographic data until now, is experimentally realized here for the first time.

References and Notes

(1) Barrer, R. M. In *Zeolites and Clay Minerals as Sorbents and Molecular Sieves*; Academic Press: New York, 1978.
(2) Breck, D. W. In *Zeolite Molecular Sieves*; Wiley: New York, 1974.
(3) Newsam, J. M. *Science* **1986**, *231*, 1093.
(4) Barrer, R. M.; Gibbson, R. M. *Trans. Faraday Soc.* **1963**, *59*, 2569.
(5) Barrer, R. M.; Vaughan, D. E. W. *Trans. Faraday Soc.* **1967**, *63*, 2275.
(6) Barrer, R. M.; Vaughan, D. E. W. *J. Phys. Chem. Solids* **1971**, *32*, 731.
(7) Barrer, R. M.; Vaughan, D. E. W. *Trans. Faraday Soc.* **1971**, *67*, 2129.
(8) Yanagida, R.; Amaro, A.; Seff, K. *J. Chem. Phys.* **1973**, *77*, 805.
(9) Jameson, C. J.; Jameson, A. K.; Gerald, R. E., II; de Dios A. C. *J. Chem. Phys.* **1992**, *96*, 1676.
(10) Jameson, A. K.; Jameson, C. J.; Gerald, R. E., II *J. Chem. Phys.* **1994**, *101*, 1775.
(11) Fraenkel, D. *J. Chem. Soc., Faraday Trans. 1* **1981**, *77*, 2029.
(12) Fraenkel, D. *J. Chem. Soc., Faraday Trans. 1* **1981**, *77*, 2041.

(13) Maienschein, J. L.; McMurphy, F. E.; Uribe, F. S. *Fusion Technol.* **1988**, *14*, 775.
(14) Penzhorn, R. D.; Leitzig, H.; Guenther, K.; Schuster, P.; Noppel, H. E. *17th DOE Nuclear Air Cleaning Conference: Proceedings*: Denver, Colorado **1983**, vol. 1, p 358−370.
(15) Heo, N. H.; Cho, K. H.; Kim, J. T. *J. Phys. Chem.* **1994**, *98*, 13328.
(16) Lim, W. T.; Chang, C. H.; Jung, K. J.; Heo, N. H. *Bull. Korean. Chem. Soc.* **2001**, *22*, 1023.
(17) Saig, A.; Danon, A.; Finkelstein, Y.; Koresh, J. E. *J. Chem. Phys.* **2003**, *118*, 4221.
(18) Danon, A.; Avraham, I.; Koresh, J. E. *Rev. Sci. Instrum.* **1997**, *68*, 4359.
(19) Amirav, A. *Org. Mass Spectrom.* **1991**, *1*, 26.
(20) Yoon, J. H.; Heo, N. H. *J. Phys. Chem.* **1992**, *96*, 4997.
(21) Jobic, H.; Bee, M.; Pouget, S. *J. Phys. Chem. B* **2000**, *104*, 7130.
(22) Kopelevic, D. I.; Chang, H. C. *J. Chem. Phys.* **2001**, *115*, 9519.
(23) Beenakker, J. J. M.; Borman, V. D.; Krylov, S. Yu. *Chem. Phys. Lett.* **1995**, *232*, 379.
(24) Wang, Q.; Challa, S. R.; Sholl, D. S.; Johnson, K. *Phys. Rev. Lett.* **1999**, *82*, 956.